Impeller posture control evaluation in 3-pole magnetic bearing for implantable pediatric ventricular assist device

Ryoichiro SATO*, Masahiro OSA*, Fumiya KITAYAMA*, Yuki NAGASAWA* and Toru MASUZAWA*
*Graduate school of Science and Engineering, Ibaraki University
4-12-1 Nakanarusawa-tyo, Hitachi-shi, Ibaraki 316-0033, Japan
E-mail: masahiro.osa.630@vc.ibaraki.ac.jp

Abstract
A maglev motor with 3-pole magnetic bearing has been developed for use in implanted pediatric ventricular assist devices (VAD). Maglev motors for implanted pediatric VAD require compact size, high magnetic suspension performance, and low power consumption due to low heat generation. However, it is difficult to achieve both high performance and efficiency in compact size maglev motors. In this paper, we developed two control methods for 3-pole magnetic bearing which are Axial position and 2-tilt angle control method and Axial position and 3-tilt angle control method. And conducted to investigate magnetic suspension performance for impeller and power consumption of the 3-pole magnetic bearing. In the result, maximum oscillation amplitudes of the impeller axial position and inclination are 0.020 mm and 0.22 deg with magnetic beating power consumption of 0.4-1.4 W and motor power consumption of 0.5-4.8 W in Axial position and 2-tilt angle control, 0.018 mm and 0.23 deg with magnetic beating power consumption of 0.4-0.6 W and motor power consumption of 0.4-1.3 W in Axial position and 3-tilt angle control. Axial position and tilt angle amplitude was sufficiently small for the axial clearance range of ±0.3 mm and the tilt angle clearance range of ±1.5 deg, resulting in equivalent magnetic support performance. Axial position and 2-tilt angle control consumed more power in motor and magnetic bearing than axial position and 3-tilt angle control. This is thought to be due to an imbalance in the motor and magnetic bearing axial attractive force. Therefore, in the future, we will create a simulation model to optimize the control and introduce zero-power control to clarify the effect of the control method on the performance of the magnetic bearings.

Keywords : Maglev, Magnetic bearing, Pediatric ventricular assist device, (Show five to ten keywords)

1. Introduction

Pediatric ventricular assist devices (VAD) have been proposed as a bridge to heart transplantation or applying adult VADs for pediatric heart failure patients. However, the only pediatric VAD currently approved in the world is the EXCOR Pediatric, an extracorporeal pulsatile flow type, developed by Bellin Heart, and the number of pediatric VADs is small (Baldwin, J. T., et al., 2006 and Ono. M., 2009). The development of an implantable and continuous-flow pediatric ventricular assist device is desired to expand the pediatric VADs and to realize home treatment. VADs based on magnetic levitation technology have been developed. The impeller of a continuous-flow blood pump is levitated by magnetic levitation technology. Durability and hemocompatibility of the blood pump can be improved by eliminating mechanical contacts (Iguchi, A., 2019, Isamu. Y., et al., 2009 and Timms, D., et al., 2008). In recent years, good clinical results of the magnetically levitated VAD HeartMate 3 (Mehra, M. R., et al., 2019) have been reported. The development of a maglev pediatric VAD is expected. Implantable pediatric VADs must be smaller than adult devices. However, the development of a magnetic levitation motor applicable to a compact pediatric blood pump is extremely difficult, and its practical application has not yet been achieved. This is because it is difficult to achieve high efficiency with a small magnetic levitation motor that has high magnetic suspension and low power consumption. Magnetic levitation motors for pediatric VADs require a 1 to 2 mm air gap for the blood gap and pump casing. In addition, the magnetic circuit of the magnetic bearing and motor must be designed to be compact enough to fit pediatric VAD. In this situation, we are

developing an implantable pediatric maglev VAD that combines a centrifugal blood pump and a magnetic levitation motor (Masuzawa, T., 2001 and Osa, M., et al., 2023). In a previous study, we develop a compact sized axial magnetic bearing with 3-poles. It was confirmed that magnetic levitation and rotation of the levitating impeller were possible by combining the developed magnetic bearing with a permanent magnet synchronous motor (Sato, R., et al., 2025). The magnetic levitation motor controlled three axes: axial direction (Z), tilt angle around X-axis and tilt angle around Y-axis. Maglev motor for pediatric VAD needs high impeller suspension performance and low power consumption. The control method may be related to magnetic suspension performance and power consumption. In the developed 3-pole magnetic bearing, the thrust poles and sensor are asymmetrically arranged on the radial axis. This may cause asymmetrical forces in the actual machine. To account this asymmetry, we added pole position gain for previous tilt angle control method which according to the geometrical arrangement of the pole positions. We defined this as Axial position and 2-tilt angle control method. And we have also developed Axial position and 3-tilt angle control method, that defines three axis (α, β, and γ) in accordance with the configuration of the X and Y axis. In this paper, we report on our investigation of magnetic suspension performance and power consumption when a prototype blood pump is driven by a maglev motor using Axial position and 2-tilt angle control method and Axial position and 3-tilt angle control method, and our study of a control method suitable for a 3-pole magnetic bearing.

2. Method

2.1. Structure of maglev motor with 3-pole magnetic bearing for pediatric VAD

The structure of the maglev motor is shown in Fig. 1. This maglev motor is an axial-gap motor in which the levitation impeller is sandwiched between a magnetic bearing and a synchronous motor. The magnetic bearing has a cylindrical pole in the center and three poles in outer side. The three outer poles are spaced at 120-degree intervals. The motor is a 6-slot and 4-pole permanent magnet synchronous motor. The yoke for the rotor and permanent magnets are placed inside the levitation impeller. The permanent magnets are placed against the magnetic bearing stator and the motor stator. On the magnetic bearing side of the levitation impeller, ring-shaped permanent magnets are arranged outside and inside. On the motor side of the levitation impeller, permanent magnets with 4-poles are arranged. The radial position of the levitation impeller is passively suspended by the magnetic coupling forces acting on the levitation impeller. The permanent magnet is made of neodymium magnet (N48H), the yoke is made of soft iron, and the stator core is made of pressed magnetic core (EU69). The number of coil turns is 123 for the motor and 181 for the magnetic bearing. The outer diameter and height of the magnetic levitation motor are 22 mm and 43 mm.

2.2. Overview of maglev and rotation control system for levitation impeller

In this magnetic levitation motor, three eddy current displacement sensors are placed at equal intervals between the magnetic bearing poles to measure the levitation impeller attitude (Fig. 2). A Hall sensor located in the slot of the motor is used to measure the speed of the levitation impeller. The position and rotation speed of the levitation impeller are calculated based on the voltage signals obtained from the eddy current displacement sensors and the Hall sensor, and the control current required for the magnetic support and rotation of the levitating impeller is determined by digital PID controller implemented in dSPACE MicroLabBox using Matlab simlink. A single-phase PWM amplifier (JUNUS, JSP 090-10) is used to excite the magnetic bearing and each coil of the motor.

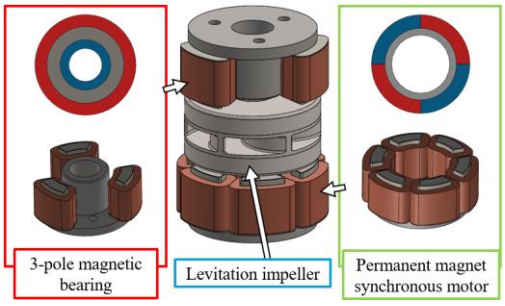

Fig. 1 Structure of maglev motor.

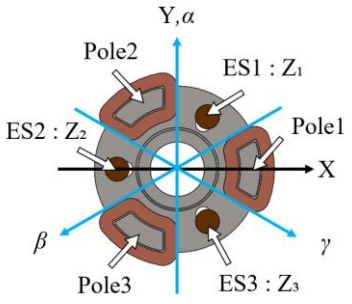

Fig. 2 Sensors, pole and axis positions.

2.3. Maglev control for levitation impeller

2.3.1. Coordinate definition of maglev motor

The positional relationship between the eddy current displacement sensor and the magnetic bearing pole is shown in Fig. 2. In this paper, each eddy current displacement sensor is defined as ES1, ES2, and ES3, and each magnetic bearing pole is defined as Pole 1, Pole 2, and Pole 3. ES1, ES2, and ES3 are located on a circle with radius r [mm] from the center of the magnetic bearing. ES1, ES2, and ES3 have a phase of 60° with respect to Pole 1, Pole 2, and Pole 3. In addition, the distances between ES1, ES2, and ES3 and the levitation impellers are defined as Z1, Z2, and Z3 [mm]. For axial position and 3-tilt angle control, three axes are defined: α, β, and γ. The α axis is on the Y axis, and β and γ axis are defined at intervals of 120 deg counterclockwise from the α axis.

2.3.2. Axial position and 2-tilt angle control method for 3-pole magnetic bearing motor

Fig. 3 shows a control overview block diagram for Axial position and 2-tilt angle control method. In this control method, the axial direction position and tilt angles around the X axis and Y axis are controlled by PID controller. The position in the magnetic direction is derived from Equation (1), the tilt angle around the X axis from Equation (2), and the tilt angle around the Y axis from Equation (3).

$$Axial = \frac{Z_1 + Z_2 + Z_3}{3} \tag{1}$$

$$Tilt\ X = \tan^{-1}\left(\frac{Z_1 - Z_3}{\sqrt{3}\cdot r}\right) \times \frac{180}{\pi} \tag{2}$$

$$Tilt\ Y = \tan^{-1}\left(\frac{(Z_1 + Z_3) - 2\cdot Z_2}{3\cdot r}\right) \times \frac{180}{\pi} \tag{3}$$

In this maglev control, the command current derived from the three PID controllers is in addition on the coils located at the three poles for excitation. As shown in Fig. 3, the axial position is suspended by the three poles, the tilt angle around the X axis by two poles (Pole2 and Pole3), and the tilt angle around the Y axis by three poles. The tilt angle control around the X and Y axes uses a different number of poles, and the pole arrangement is geometrically different. Therefore, in order to avoid excess torque around the X and Y axis and excess attractive force in the axial direction, the command value derived from each PID controller is multiplied by a position gain for each of the individual poles. The excitation currents $i_{Pole\,1}$, $i_{Pole\,2}$, and $i_{Pole\,3}$ to the coils installed at each pole can be expressed as Equation (4) from the command i_{Axial}, $i_{Tilt\,X}$, and $i_{Tilt\,Y}$ from the PID controllers and the pole position gain.

$$\begin{bmatrix} i_{Pole\,1} \\ i_{Pole\,2} \\ i_{Pole\,3} \end{bmatrix} = \begin{bmatrix} 1 & 0 & \frac{4}{3} \\ 1 & \frac{2}{\sqrt{3}} & -\frac{2}{3} \\ 1 & -\frac{2}{\sqrt{3}} & -\frac{2}{3} \end{bmatrix} \begin{bmatrix} i_{Axial} \\ i_{Tilt\,X} \\ i_{Tilt\,Y} \end{bmatrix} \tag{4}$$

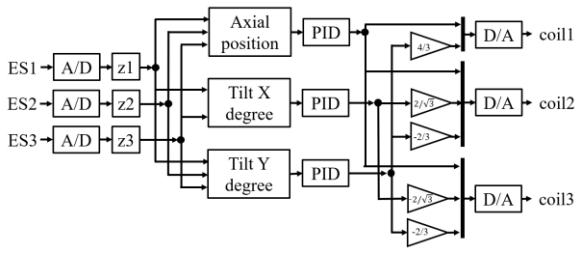

Fig. 3 Block diagram of Axial position and around 2-tilt axis control method.

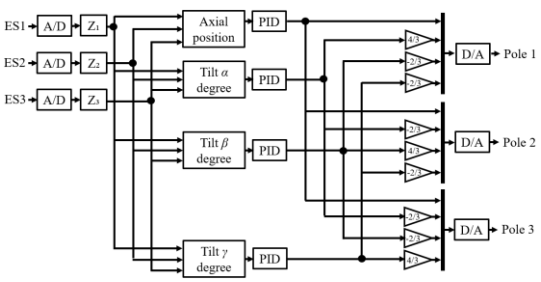

Fig. 4 Block diagram of Axial position and around 3-tilt axis control method.

Define k as the force coefficient (N/A) of one pole and R as the distance from the center to the pole position. The axial position can be expressed as in Equation (5), since the same force is applied from the three poles. Torque is expressed as Equation (6), since it is necessary to consider the pole positions. Substituting the commanded currents to the poles derived from equation (4) into equation (6), it can be confirmed that the torque coefficients around the X and Y axis are same.

$$F_z = 3ki_{Axial} \tag{5}$$

$$\begin{bmatrix} T_X \\ T_Y \end{bmatrix} = kR \begin{bmatrix} 0 & \frac{\sqrt{3}}{2} & -\frac{\sqrt{3}}{2} \\ 1 & -\frac{1}{2} & -\frac{1}{2} \end{bmatrix} \begin{bmatrix} i_{Pole\,1} \\ i_{Pole\,2} \\ i_{Pole\,3} \end{bmatrix} \tag{6}$$

2.3.3. Axial position and 3-tilt angle control method for 3-pole magnetic bearing motor

Fig. 4 shows a control overview block diagram for Axial position and 3-tilt angle control method. In this control method, the axial direction position and tilt angles around the α, β, and γ axes are controlled by PID control. The position in the magnetic direction is derived from Equation (1), and the tilt angle around the α, β, and γ axes is derived from Equations (7)-(9). The derivation of the tilt angle around the αaxis is the same as the derivation of the tilt angle around the Y axis. For the β and γ axes, the tilt angles are derived from three eddy current displacement sensors at positions shifted by 120 deg, as in the case of the Y axis. This is thought to allow the actual machine to detect the tilt angle with higher accuracy than around the X axis.

$$Tilt\ \alpha = \tan^{-1}\left(\frac{(Z_1 + Z_3) - 2 \cdot Z_2}{3 \cdot r}\right) \times \frac{180}{\pi} \tag{7}$$

$$Tilt\ \beta = \tan^{-1}\left(\frac{(Z_2 + Z_1) - 2 \cdot Z_3}{3 \cdot r}\right) \times \frac{180}{\pi} \tag{8}$$

$$Tilt\ \gamma = \tan^{-1}\left(\frac{(Z_3 + Z_2) - 2 \cdot Z_1}{3 \cdot r}\right) \times \frac{180}{\pi} \tag{9}$$

Fig. 4 shows that in this control method, the coils placed on each of the rams are excited by adding up the command values derived from the PID controller for the tilt angle around the axial direction and the α, β and γ axis. The tilt angle control around theα, β and γ axis is also multiplied by the pole position gain in the same way as the tilt angle control around the Y axis. This suppressed the disturbance in the axial direction. The excitation currents $i_{Pole\,1}$, $i_{Pole\,2}$, and $i_{Pole\,3}$ to the coils installed at each pole can be expressed as Equation (10) from the commands i_{Axial}, $i_{Tilt\,\alpha}$, $i_{Tilt\,\beta}$, and $i_{Tilt\,\gamma}$ from the PID controller and the pole position gain. The axial pull force and tilt torque in this control method can be derived by substituting the result of Equation (10) into Equations (5) and (6) same as in Section 2.3.3.

$$\begin{bmatrix} i_{Pole\,1} \\ i_{Pole\,2} \\ i_{Pole\,3} \end{bmatrix} = \begin{bmatrix} 1 & \frac{4}{3} & -\frac{2}{3} & -\frac{2}{3} \\ 1 & -\frac{2}{3} & \frac{4}{3} & -\frac{2}{3} \\ 1 & -\frac{2}{3} & -\frac{2}{3} & \frac{4}{3} \end{bmatrix} \begin{bmatrix} i_{Axial} \\ i_{Tilt\,\alpha} \\ i_{Tilt\,\beta} \\ i_{Tilt\,\gamma} \end{bmatrix} \tag{10}$$

2.3.4. Determination of tilt PID controller gain for control methods

In the magnetic suspension of the levitation impeller, the command current of axial position control is the same for Axial position and 2-tilt control method and Axial position and 3-tilt control method. However, the control variable in the tilt PID control system is different for Axial position and 2-tilt control method and Axial position and 3-tilt control method. However, Axial position and 2-tilt control method and Axial position and 3-tilt control method have different control quantities in the inclined PID control system. We consider a PID controller so that the control currents excited at each pole are equal for any given levitating impeller attitude, regardless of the difference in the control variable. Equation

11 shows the equation for converting the tilt angle around the X and Y axis to the α, β and γ axis, assuming that the PID gains of the tilt angle control controller around the X and Y and α, β and γ axes are similar. Consider the case where the impeller is tilted by an arbitrary angle θ deg around the X axis and Y axis. In this case, derive the excitation current from equations (4) and (10), substitute it into equation (6), and derive the tilt torque around the X axis and Y axis. The result shows that Axial position and 3-tilt control method can generate 1.5 times the torque of Axial position and 2-tilt control method. Therefore, the tilt angle control PID controller gain around the X and Y axis needs to be 1.5 times the tilt control PID controller gain around the α, β and γ axis. This results in the same command current for the same error.

$$\begin{bmatrix} Tilt\ \alpha \\ Tilt\ \beta \\ Tilt\ \gamma \end{bmatrix} = \begin{bmatrix} 0 & 1 \\ \frac{\sqrt{3}}{2} & -\frac{1}{2} \\ -\frac{\sqrt{3}}{2} & -\frac{1}{2} \end{bmatrix} \begin{bmatrix} Titt\ X \\ Tilt\ Y \end{bmatrix} \tag{11}$$

2.4. Performance investigation test of a maglev motor using a prototype blood pump

Axial position and 2-tilt control method and Axial position and 3-tilt control method were applied to a magnetically levitated blood pump to compare magnetic suspension and power consumption performance. Table 1 shows the PID controller gains for Axial position and 2-tilt control method, and Axial position and 3-tilt control method. The PID controller gains for the levitation control were determined by trial-and-error method under the conditions of 4000 rpm and 1.5 L/min flow rate, which are target pump operating points, when operating with Axial position and 3-tilt control method. control method, the controller gains for the levitation control were determined by referring to the gains calculated by the method described in section 2.3.4. The PI controller gains for the synchronous motor rotation control were the same regardless of the levitation control method. A prototype blood pump made of resin shown in Fig. 5(b) was connected to the closed loop simulated circulatory circuit filed by water shown in Fig. 5(a) for the experiment. The clearance range of the impeller in this blood pump is ±0.3 mm in the axial direction position and ±1.5 deg in the tilt angle. The rotational speed was set at 3000-5000 rpm, which is the expected operating range of this blood pump for pediatric ventricular assist device. The flow rate increased from 0 L/min to 0.5 L/min in increments by operating the pinchcock valve. The flow rate was measured with an ultrasonic flow meter. Head pressure was measured from the difference between strain-gauge pressure gauges installed at the pump inlet and outlet. Power consumption was measured with a digital power meter. The sampling frequency and control frequency of the magnetic levitation and rotation control system were set to 10 kHz. The axial position and tilt angle of the levitating impeller were measured for 1 second, and half of the difference between the maximum and minimum values in the measured data was used as the amplitude.

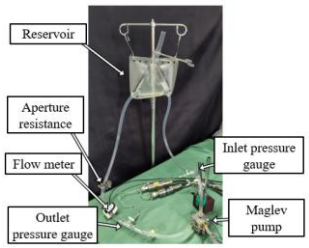

(a) Closed loop circulation circuit.

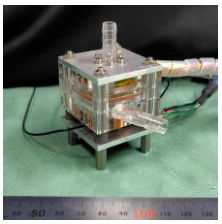
(b) Prototype maglev blood pump.

Fig. 5 Experimental device for performance investigation test.

Table 1 PID controller gain.

	P	I	D
Axial position	10 [A/mm]	0.5 [A/sec mm]	0.18 [A sec/mm]
Tilt X, Y	0.975 [A/deg]	0.015 [A/sec deg]	0.00225 [A sec/deg]
Tilt α, β, γ	0.65 [A/deg]	0.01 [A/sec deg]	0.0015 [A sec/deg]
Rotation control	0.0005 [A/rpm]	0.0018 [A/sec rpm]	0 [A sec/rpm]

3. Result

The results when Axial position and 2-tilt angle control method is used for attitude control of the levitating impeller are shown as solid lines, while the results when Axial position and 3-tilt angle control method is used are shown as dashed lines (Fig. 6-9). The HQ characteristics of the magnetic levitation blood pump are shown in Fig. 6. At all pump operating points, there was no difference in HQ characteristics depending on the control method. The developed blood pump was able to adjust the auxiliary flow rate in the range of 0-3 L/min for a head of 60-100 mmHg.

The amplitudes of Z1, Z2, and Z3 at 3000, 4000, and 5000 rpm and the average axial amplitudes calculated from equation (1) are shown in Fig. 7 (a)-(d) The amplitudes of Z1, Z2, and Z3 in Axial position and 2-tilt angle control were 0.027-0.038 mm at 3000 rpm (Fig. 7 (a)) and 0.021-0.037 mm at 4000 rpm (Fig. 7 (b)), and 0.022-0.032 mm at 5000 rpm (Fig. 7 (c)).The amplitudes of Z1, Z2, and Z3 of Axial position and 3-tilt angle control were 0.029-0.038 mm at 3000 rpm (Fig. 7 (a)), 0.025-0.035 mm at 4000 rpm (Fig. 7 (b)), and 0.024-0.035 mm at 5000 rpm (Fig. 7 (c)). The average axial amplitudes were 0.009-0.20 for Axial position and 2-tilt angle control and 0.007-0.034 for Axial position and 3-tilt angle control at 3000-5000 rpm (Fig. 7 (d)). The axial amplitudes were smaller at 4000 and 5000 rpm than at 3000 rpm.. Z1, Z2, Z3, and the average value were all very small compared to the clearance range of ±0.3 mm. Z1, Z2 and Z3 amplitudes were similar for both Axial position and 2-tilt angle control method and Axial position and 3-tilt angle control method control methods. The average axial amplitude of Axial position and 3-tilt angle control was slightly smaller than that of Axial position and 2-tilt angle control.

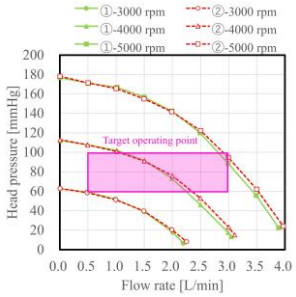

Fig. 6 HQ characteristic.

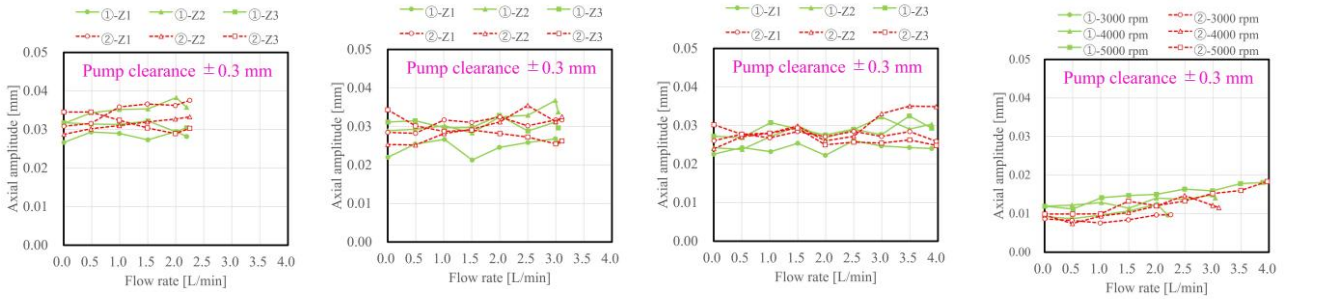

(a) 3000 rpm Z amplitude. (b) 4000 rpm Z amplitude. (c) 5000 rpm Z amplitude. (d) Axial position amplitude.

Fig. 7 Axial position amplitude.

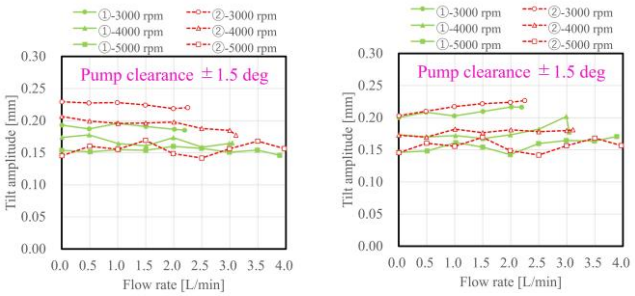

(a) Tilt X angle amplitude. (b) Tilt Y angle amplitude.

Fig. 8 Tilt angle amplitude.

The tilt angle amplitudes around the floating impeller X and Y axes calculated from Equations (2) and (3) for both control methods are shown in Figs. 8 (a) and (b). At 3000, 4000, and 5000 rpm, the tilt angle amplitude around the X axis in Axial position and 2-tilt control was 0.15-0.20 deg (Fig. 8 (a)) and that around the Y axis was 0.14-0.22 deg (Fig. 8 (b)). In Axial position and 3-tilt control, the tilt angle amplitude around the X axis was 0.16-0.23 deg (Fig. 8 (a)), and that around the Y axis 0.14-0.23 deg (Fig. 8 (b)). In both cases, the tilt angle amplitude decreased with increasing rotation speed. And the tilt angle amplitude was sufficiently small for a motion range of ±1.5 deg regardless of both control methods. In case of Axial position and 3-tilt control, the tilt angle amplitude around the Y axis was smaller than that around the X axis. In Axial position and 2-tilt control, the tilt amplitude was the same around the X axis and Y axis, and the tilt amplitude of Axial position and 2-tilt angle control was slightly smaller than that of Axial position and 3-tilt angle control at 3000 and 4000 rpm around the X axis.

Fig. 9 (a) and (b) show the power consumption of the pump drive in 3000-5000 rpm. Fig. 9 (a) shows the power consumption of the magnetic bearing and Fig. 9 (b) shows the power consumption of the motor. The power consumption of the magnetic bearing in Axial position and 2-tilt angle control is 0.39-1.44 W (Fig. 9 (a)) and that of the motor is 0.46-4.82 W (Fig. 9 (b)). The magnetic bearing power consumption of Axial position and 3-tilt angle control was 0.36-0.61 W (Fig. 9 (a)) and the motor power consumption was 0.44-4.32 W (Fig. 9 (b)). The magnetic bearing and motor power consumption of Axial position and 2-tilt angle control was larger than that of Axial position and 3-tilt angle control. The larger the rotation speed, the larger the difference in power consumption between Axial position and 2-tilt angle control and Axial position and 3-tilt angle control.

4. Discussion

A blood pump was driven noncontact by a magnetic levitation motor with axial magnetic bearings, and it was capable of pumping more than 2.5 L/min for a pump head of 60-100 mmHg. Since there was no difference in HQ characteristics due to the control method, it is considered that the experiments could be performed under similar operating conditions. The research and development of the small magnetic levitation motor in this study will contribute to the realization of an implantable pediatric ventricular assist device with high durability and hemocompatibility.

Both control methods showed sufficient suppression control performance for a maglev motor used in a pediatric VAD. The axial amplitudes of Z1, Z2, and Z3 and the average axial amplitude results show that the levitation impeller was in processional motion with both control methods. Equivalent results were expected for axial amplitudes because similar control methods were used. However, the axial amplitude of A was slightly larger than that of B. This is because the motor generated an axial disturbance. Tilt angle errors occur similar command currents in tilt angle controllers, so we expected equivalent tilt X and Y angle amplitudes in both control methods. However, Axial position and 3-tilt angle control's amplitude around the X axis was slightly larger than Axial position and 2-tilt angle control. This is because the comparison of Axial position and 2-tilt angle control and Axial position and 3-tilt angle control methods in Chapter 2 is simplified and does not consider some points. The axial amplitude and tilt angle amplitude became smaller as the rotation speed increased. And the difference in tilt angle amplitude by control method became smaller as the rotation speed increased. However, there was no significant change in axial amplitude. This is because an increase in levitation impellers rotational speed provides a restoring force due to the gyro moment, and water fluid in the pump acts as a damper to suppress the tilt amplitude. These results show that the magnetic suspension performance is almost the same for both control methods because the command current of the control is equalized by PID gains.

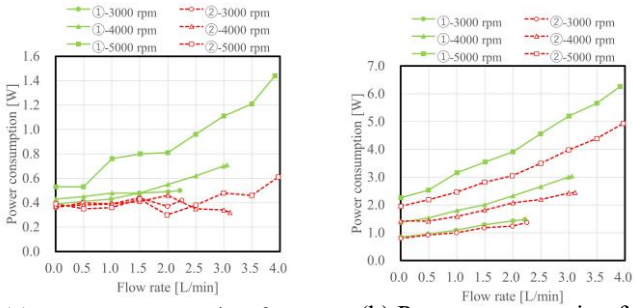

(a) Power consumption for magnetic suspension.

(b) Power consumption for rotation.

Fig. 9 Power consumption.

Magnetic bearing with Axial position and 2-tilt angle control and motor power consumption increased with increasing flow rate and speed. However, the magnetic bearing power consumption in Axial position and 3-tilt angle control was constant regardless of the drive conditions. In Axial position and 2-tilt angle control, the motor consumed more power than in Axial position and 3-tilt angle control. This was caused by a phase shift in the motor control with Axial position and 2-tilt angle control. Phase shift in motor control triggers extra axial attraction. This extra axial attractive force increased extra axial attractive force and power consumption in the magnetic bearing. This is the reason why the power consumption of the magnetic bearings in the Axial position and 2-tilt angle control is larger than in the Axial position and 3-tilt angle control. Therefore, it is possible to reduce the power consumption of the magnetic bearing and motor at Axial position and 2-tilt angle control by introducing zero-power control to the axial direction control in the future. Introducing zero-power control could lead to reduced power consumption not only in Axial position and 2-tilt angle control but also in Axial position and 3-tilt angle control. Another possibility for reducing power consumption is a control system that applies the optimum gain according to the pump drive situation.

5. Conclusion

We developed two attitude control methods for levitating impellers with 3-pole magnetic bearings that are Axial position and 2-tilt angle control method and Axial position and 3-tilt angle control method. Then, we investigated magnetic suspension and power consumption for the two developed control methods. As a result, the magnetic suspension performance of the levitating impeller was better for the tilt angle around the X axis with Axial position and 2-axis tilt angle control suppressing vibration better than Axial position and 3-tilt angle control. And the suspension performance of the axial position and Y axis tilt angles was equivalent. The power consumption by Axial position and 3-tilt angle control was smaller than that of Axial position and 2-tilt angle control. Based on these results, it is unclear what kind of force is generated by the magnetic suspension in the actual machine. For this reason, we will develop a simulation model of a magnetic bearing and optimize the control gains for Axial position and 2-tilt angle control and Axial position and 3-tilt angle control method. And we will also investigate the details of the dynamic characteristics of the attitude control of the levitating impeller when a disturbance is applied by excitation for each control method.

References

Baldwin, J. T., Borovetz, S. B., Duncan, B. W., Gartner, M. J., Jarvik. R. K., and Weiss, W. J. The National Heart, Lung, and blood Institute Pediatric Circulatory Support, Journal of the American heart association (2006), pp. 147-155.

Iguchi, A., Progress in Artificial Heart, Artificial organs (2019) , Vol. 48, No. 3, pp. 144- 146.

Isamu Y., Aly E., Masataka Y., Mitsumasa H., Akira S., Tetsuya N., Shinji W., Reiner K., and Kazutomo M., First Clinical Application of the DuraHeart Centrifugal Ventricular Assist Device for a Japanese Patient, Artificial Organs (2009), Vol. 33, No. 9, pp. 763-766.

Masuzawa, T., Design of Implantable Artificial Heart, Design Engineering, Japan Society for Design Engineering (2001), Vol. 36, No. 7, pp. 1-13 (in Japan).

Ono. M., Current Status and Prospects of the Assistive Artificial Heart. Pediatrics (2009), Vol. 42, No. 5, pp. 36-37 (in Japan).

Mehra, M. R., Uriel, N., Naka, Y., et al., A Fully Magnetically Levitated Left Ventricular Assist Device Final Report, N Engl J Med 2019 (2019), Vol. 380, pp. 1618–1627.

Osa, M., Masuzawa, T., Kitayama, F., Nishinaka, T., and Tatsumi, E., A Magnetically Suspended Pediatric Ventricular Assist Device with a Multi-Degrees of Freedom Controlled Self-Bearing Motor Using a Simplified Driving System, Journal of the Japan Society of Applied Electromagnetics and Mechanics (2023), Vol. 31, No. 2, pp. 257-263 (in Japan).

Sato, R., Osa, M., Kitayama, F., and Masuzawa, T., Effects of Control Methods on the Stability of 3-Pole Magnetic Bearing, Journal of the Japan Society of Applied Electromagnetics and Mechanics (2025), Vol. 33, No. 2, pp. 66-73 (in Japan).

Timms, D., Fraser, J., Hayne, M., Dunning, J., McNeil, K., and Pearcy, M., The BiVACORE Rotary Biventricular Assist Device : Concept and In Vitro Investigation, Artificial Organs (2008), Vol. 32, No. 10, pp. 757-829.